metals

MDPI

Article

Flow Stress Behaviour and Static Recrystallization Characteristics of Hot Deformed Austenite in Microalloyed Medium-Carbon Bainitic Steels

Pentti M. Kaikkonen *, Mahesh C. Somani, Leo Pentti Karjalainen and Jukka I. Kömi

Materials and Mechanical Engineering, Centre for Advanced Steels Research, University of Oulu, 90014 Oulun yliopisto, Finland; mahesh.somani@oulu.fi (M.C.S.); pentti.karjalainen@oulu.fi (L.P.K.); jukka.komi@oulu.fi (J.I.K.)

* Correspondence: pentti.kaikkonen@oulu.fi; Tel.: +358-440-172-490

Abstract: In the past decade, efforts have been focused on developing very fine, medium-carbon bainitic steels via the low-temperature (typically 300–400 °C) ausforming process, which not only enables shorter isothermal holding times for bainitic transformation at low temperatures, but also offers significantly improved strength. This paper describes static recrystallization (SRX) characteristics of austenite in four medium-carbon 2%Mn-1.3%Si-0.7%Cr steels with and without microalloying intended for the development of these steels. The stress-relaxation method on a Gleeble simulator resulted in recrystallization times over a wide range of temperatures, strains and strain rates. Also, the occurrence of precipitation was revealed. Powers of strain (−1.7 to −2.7) and strain rate (−0.21 to −0.28) as well as the apparent activation energies (225–269 kJ/mol) were in the ranges reported in the literature for C-Mn and microalloyed steels with lower Mn and Si contents. The new regression equations established for estimating times for 50% SRX revealed the retardation effects of microalloying and Mo addition showing reasonable fits with the experimental data, whereas the previous model suggested for ordinary microalloyed steels tended to predict clearly shorter times on average than the experimental values for the present coarse-grained steels. The Boratto equation to estimate the non-recrystallization temperature was successfully modified to include the effect of Mo alloying and high silicon concentrations.

Keywords: medium-carbon steels; austenite; flow stress; stress relaxation; recrystallization kinetics; precipitation

Citation: Kaikkonen, P.M.; Somani, M.C.; Karjalainen, L.P.; Kömi, J.I. Flow Stress Behaviour and Static Recrystallization Characteristics of Hot Deformed Austenite in Microalloyed Medium-Carbon Bainitic Steels. *Metals* **2021**, *11*, 138. https://doi.org/10.3390/met11010138

Received: 21 December 2020
Accepted: 8 January 2021
Published: 12 January 2021

1. Introduction

Nanostructured bainite, also called superbainite, is a novel type of microstructure for creating modern tool and construction steels exhibiting exceptional durability [1]. Recently, efforts have been focused on developing very fine, medium-carbon bainitic steels by introducing a low-temperature (typically 300–400 °C) ausforming process, thus facilitating a very fine nanostructured bainitic structure in the steels [2–5]. Not only does the low temperature deformation offer improved strength, but it also enables shorter isothermal holding times for the completion of bainitic transformation at a given temperature. A careful alloy design is, therefore, necessary as a low martensite start temperature M_S must be obtained. This is possible typically by the addition of austenite stabilizing elements such as Mn. Additions of Mo and microalloying elements V and Nb are quite usual in order to utilize their grain refinement and strengthening effects on the final bainitic microstructure. On the other hand, Si addition in suitable quantities hinders the undesirable formation of carbides during low temperature (typically 300–400 °C) isothermal holding and helps stabilize a fraction of finely divided, carbon-enriched retained austenite (RA) at room temperature (RT) during final cooling. While a nanostructured bainitic matrix has the potential to provide the required ultrahigh strength, a small fraction of RA finely divided

between the bainitic laths is expected to provide improved work hardening and uniform elongation without a loss of impact toughness.

In addition to the composition design, hot rolling in the recrystallization regime, i.e., above the no-recrystallization temperature T_{nr}, is an essential stage in terms of refinement of the austenite grain size prior to low temperature ausforming. Also, the characteristics and kinetics of precipitation in the steels, if any, need to be understood in order to complete the recrystallization process prior to its occurrence. An appropriate control of the hot rolling sequence in accord with the static recrystallization (SRX) characteristics and kinetics is, therefore, inevitably necessary.

The SRX kinetics of hot deformed austenite in C-Mn steels (with Mn < 1.5%, Si < 0.25%; hereinafter, all concentrations are in wt.%) as a function of chemical composition including the effects of V, Ti and Nb have been reported by numerous authors, for example, [6–12]. Medina and Quispe [13] have published experimental recrystallization-precipitation-time-temperature diagrams for various V and Nb microalloyed steels illustrating the start and finish temperatures of SRX as well as precipitation at different temperatures. Garcia-Mateo et al. [8] reported retardation of SRX kinetics due to the addition of 0.18 and 0.24% V in a C-Mn steel. Furthermore, they pointed out the mechanisms that discretely caused the retardation at low as well as high temperatures; the solute drag effect being the main reason at high temperatures and the presence of fine precipitates at low temperatures. Vervynckt et al. [9] also examined the influence of different levels of Nb-microalloying on the SRX kinetics in low-carbon steels at 900 °C, and according to their study, 0.02% Nb alloying caused delay in the SRX kinetics only due to the solute drag effect, whereas a higher Nb alloying (0.04–0.16% Nb) resulted in both precipitation as well as the solute drag effect, respectively. The hindering effect of V and Nb on SRX kinetics in low alloy steels was also reported by Esterl et al. [10]. Pereda et al. [11] concluded that increasing Mo content in 0.05C-Nb steels increased the T_{nr} essentially due to an enhanced solute drag effect in steels with low Nb content (0.03% Nb), whereas in steels with relatively higher Nb content (0.06% Nb), the acceleration of strain induced precipitation became more relevant than the solute drag.

In general, the time for 50% SRX fraction (t_{50}) can be described by the following empirical relation [14,15]:

$$t_{50} = A\, \varepsilon^{p}\, \varepsilon'^{q}\, d^{s}\, \exp(Q_{app}/\mathrm{RT}) \quad (1)$$

where A, p, q and s are material dependent constants, ε is strain, ε' is strain rate, d is initial grain size and Q_{app} is the apparent activation energy of static recrystallization. R is the universal gas constant and T is the absolute temperature. Generally, the double-hit deformation technique has been used for determining the powers of the variables in Equation (1) after compression or torsion deformation, for example, [16–20]. However, stress relaxation testing has been shown to be a very effective and reliable technique in determining the SRX and metadynamic recrystallization (MDRX) kinetics, because a single stress relaxation experiment can provide a complete restoration curve describing the recrystallized fraction versus holding time for a given set of conditions [16,17]. Also, the recovery and recrystallization processes can be distinguished [16]. Somani et al. [18,21–23] developed a comprehensive regression model to predict the kinetics of SRX for hot-deformed austenite based on the stress relaxation test results for over 40 different carbon steels. The model is able to satisfactorily predict the SRX kinetics of common carbon steel grades including microalloyed steels and also several special steel grades. During the development of this model, the influence of alloying with Mn in the range 0.02–2% and Si up to 1.5% alloying was also considered by including the instances of a couple of dual-phase and **t**ransformation **i**nduced plasticity (TRIP) steels. Although a large number of steels were found to obey a simple relationship, certain alloying elements such as Si, resulted in differences and an upper saturation limit had been successfully considered [18,24]. The maximum concentration of Nb too seemed to be limited to fit the common relationship and likewise, an upper saturation limit was considered [18]. Recently, the effects of Si and Mn on recrystallization characteristics of high-Si steels have also been investigated [25].

In V, Ti and Nb-microalloyed steels, strain-induced precipitation tends to occur at low rolling temperatures close to T_{nr}, and a drop in stress with time, normally seen during relaxation, may halt or even increase for some duration, so that the relaxation testing technique can also be used to determine the start (P_s) and finishing time (P_f) of precipitation corresponding to the stop and restart of relaxation process, respectively [6,26–29]. The occurrence of precipitation in various steels, microalloyed with Ti and Ti-V [12], as well as V, Ti, Nb [6,26,29–32], have been investigated by the stress relaxation technique.

Optimization of the thermomechanical processing can be done with the aid of physical simulation studies. In the present work, the chosen approach was to design the appropriate processing conditions for select medium-carbon compositions considered suitable for low-temperature ausforming and subsequent fine-grained bainite formation. However, determining the SRX behaviour of these steels was the main target of the present study in order to be able to finetune the hot rolling processes prior to cooling and low temperature ausforming. The aim is to understand the effects of supplementary additions of V and Mo on the SRX characteristics and kinetics of Nb-microalloyed, medium carbon steels with high-Mn/Si ((0.4–0.5)C-2Mn-1.3Si). Notably, many regression equations describing the effects of microalloying on the SRX rates already exist in the literature for conventional low-carbon steels, as mentioned above and also listed by Lenard et al. [33]. Owing to significant scatter in predictions using these equations, this study further aims to re-examine the potential roles of V-Nb and Mo-Nb alloying in medium-carbon steels with high Mn and Si contents, particularly in the light of the previous model developed at the authors' laboratory [18,21–23]. The well-known equations from Barbosa et al. [34] and Bai et al. [35] for estimating T_{nr} were realised to give unreliable results for the present steels, so this study also proposes a modification of the equation, to include the effect of Mo.

2. Materials and Methods

Four medium-carbon 2Mn-1.3Si steels designed for achieving nanostructured bainite, coded Mn-Si, Mo-Nb, V-Nb and C-V-Nb with varying C, Mo, V and Nb alloying, were the experimental materials in this study for the characterization of flow stress and SRX behaviours. All steels were received in the form of homogenized and hot rolled 12 mm thick plates from OCAS, Ghent, Belgium. The chemical compositions of the steels are shown in Table 1. The prior austenite grain sizes (PAGS) of the steels, measured using the linear intercept method according to ASTM E112-12 standard on specimens austenitized at the reheating temperature 1250 °C for 2 min, followed by quenching with water spray to room temperature (RT) and etched in 2% Nital solution, are also included in Table 1.

Table 1. Chemical compositions of the steels in wt.-% (Fe balance) and prior austenite grain sizes (PAGS).

Steel Code	C	Si	Mn	Cr	Mo	V	Nb	PAGS (μm)
Mn-Si	0.39	1.4	2.0	0.7	<0.01	0.02	<0.01	650
Mo-Nb	0.40	1.3	2.0	0.7	0.30	0.02	0.026	461
V-Nb	0.40	1.3	2.0	0.7	<0.01	0.10	0.018	417
C-V-Nb	0.48	1.3	2.0	0.7	<0.01	0.10	0.021	401

N in the range of 20–45 ppm, S: 10–20 ppm, P: 30–50 ppm.

Cylindrical specimens of dimensions, Ø10 × 12 mm, were machined from the plates for stress relaxation testing with the axis transverse to the rolling direction. The tests were conducted in a Gleeble 3800® (Dynamic Systems Inc., Poestenkill, NY, USA) thermomechanical simulator. A tantalum foil was used to prevent sticking of samples to the tungsten carbide anvils and a graphite foil was used as a lubricant between the tantalum foil and the anvils.

The specimens were heated at a constant rate of 10 °C/s to the reheating temperature of 1250 °C, held for 2 min, followed by cooling at 2 °C/s to the deformation temperature, where the specimens were first held for 15 s to stabilize the temperature prior to compression and stress relaxation. Subsequently, the samples were compressed to a prescribed

strain at a particular strain rate, followed by stress relaxation for 200–600 s in the stroke mode, where the compressive force was relaxed by keeping the strain constant during the course of holding. However, a very small strain rate of about 0.0003 s^{-1} had to be applied during holding in order to maintain electrical contact between the specimen and the anvils. The stress was recorded as a function of the time during holding, and the relaxation curve fitted with an Avrami-type (JMAK) equation for determining t_{50} in order to obtain the SRX fraction as a function of holding time t [36,37]

$$X = 1 - \exp(-0.693(t/t_{50})^n) \quad (2)$$

where n is the Avrami (JMAK) exponent. Tests were carried out in the deformation temperature (T_{Def}) range 900–1200 °C corresponding to the hot rolling regime and also, the strain (0.125–0.4) and strain rate (0.01–5 s^{-1}) were suitably varied over wide ranges in order to determine the SRX characteristics and respective material constants. A schematic illustration of the experiment schedule is shown in Figure 1a and the corresponding experimental setup showing a sample between the anvils just before deformation in the Gleeble simulator is presented in Figure 1b. Detailed test conditions are presented in Table 2.

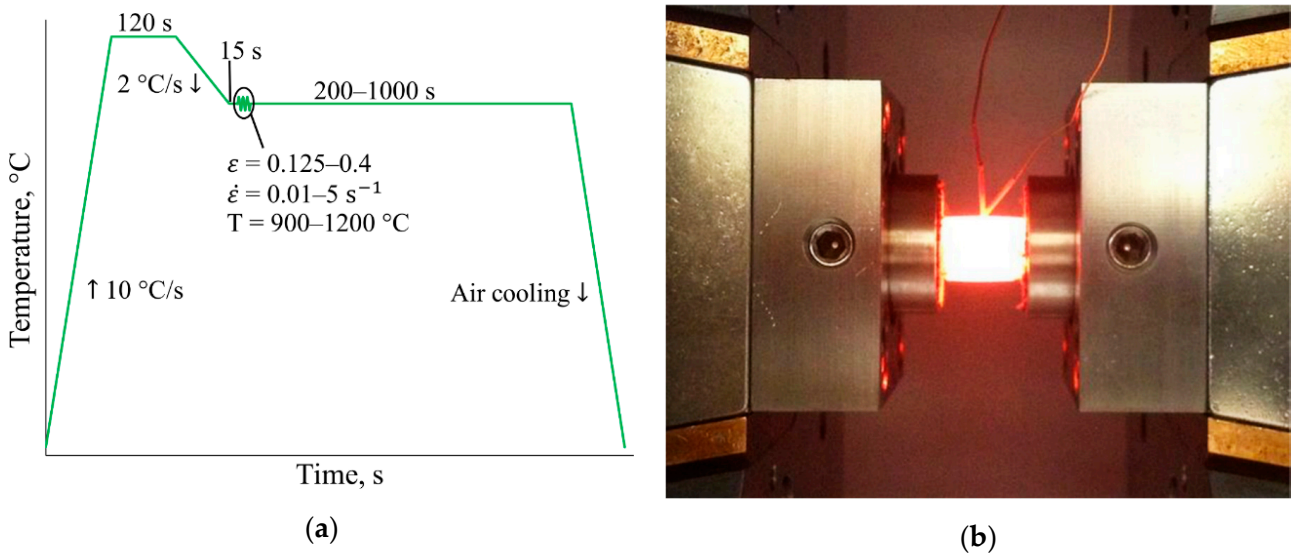

Figure 1. (**a**) Schematic of stress-relaxation test schedules, (**b**) experimental setup in the initial state (prior to deformation).

For the Nb-microalloyed steels, the suitable reheating temperatures were determined using the Thermo-Calc software (version 2019a, Thermo-Calc Software AB, Solna, Sweden) with the Precipitation module (TC-PRISMA), with the objective to dissolve all of the 0.026% of Nb into the solid solution. The critical solution temperatures of NbC were found to be 1220 °C and 1235 °C for 0.4% steel and 0.5% C-bearing steel respectively (see Figure 2). In addition, the reheating temperature (T_{RH}) and/or time (t_{RH}) of all the steels were aptly varied (Table 2) to produce relatively finer grain structures in order to determine the influence of grain size on SRX kinetics and check the validity of the empirical equations for fractional softening.

Table 2. Test conditions for the medium-carbon steels.

Steel Code	T_{RH} (°C)/t_{RH} (min)	PAGS (μm)	T_{Def} (°C)	Strain	Strain Rate (s^{-1})
Mn-Si	1250/2	650	900, 950, 1000, 1050, 1150, 1200	0.2	0.1
			1050	0.125–0.4	0.1
			1050	0.2	0.01–5
	1250/1	132	1000, 1050, 1100	0.2	0.1
			1050	0.15–0.35	0.1
	1150/2	121	1050	0.2	0.1
Mo-Nb	1250/2	461	900, 950, 1000, 1075, 1125, 1150, 1175, 1200	0.2	0.1
			1100	0.125–0.4	0.1
			1100	0.2	0.01–5
	1250/1	195	1000, 1050, 1100	0.2	0.1
			1050	0.15–0.35	0.1
	1150/2	157	1050	0.2	0.1
V-Nb	1250/2	417	900, 950, 1000, 1050, 1150, 1200	0.2	0.1
			1050	0.125–0.4	0.1
			1050	0.2	0.01–5
	1250/1	207	1000, 1100	0.2	0.1
			1050	0.15–0.35	0.1
C-V-Nb	1250/2	401	900, 950, 1000, 1050, 1125, 1150, 1200	0.2	0.1
			1050	0.125–0.4	0.1
			1050	0.2	0.01–5
	1150/1	154	1050	0.2	0.1

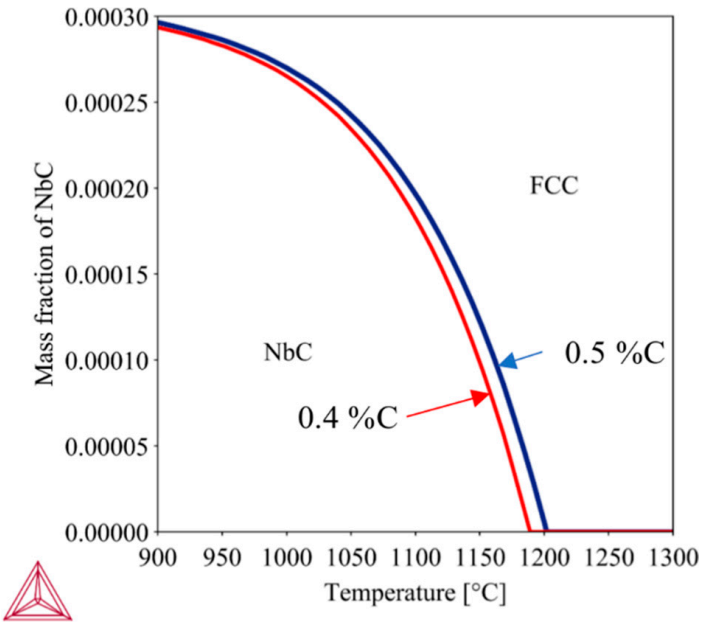

Figure 2. Mass fraction of NbC in equilibrium condition calculated with TC-PRISMA.

3. Results and Discussion

3.1. Flow Stress Behaviour

Examples of typical true stress-true strain curves for the Mn-Si and Mo-Nb steels reheated at 1250 °C/2 min and compressed to a true strain of ~0.2 at a constant true strain rate of 0.1 s^{-1} in the temperature range of 900–1200 °C are shown in Figure 3,

illustrating typical flow stress behaviour of the steels prior to stress relaxation. The shape of the flow stress curves suggests work hardening and dynamic recovery processes at all deformation temperatures. Thus, relaxation after hot compression should characterize the static restoration (recovery and recrystallization) processes, except presumably at 1150–1200 °C, where the critical strain for the onset of dynamic recrystallization (≈0.8 times peak strain) might be very close or exceeded [15,38], even though the peak strain was not determined (and not reached yet). Flow stress behaviour of such cases, in which the borderline situation of static and MDRX was suspected, was carefully examined in order to exclude them while modelling the fractional softening equations for SRX. Similarly, those cases, where recrystallized fractions after relaxation were clearly partial, were excluded from developing the empirical equations.

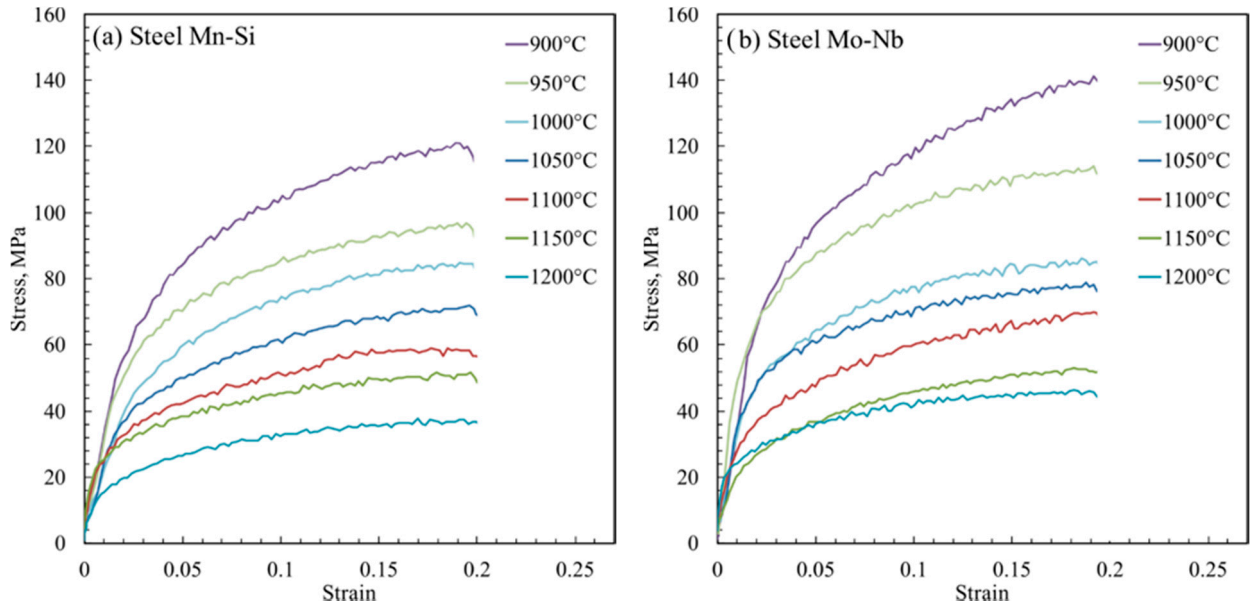

Figure 3. Typical true stress–true strain curves during hot compression to 0.2 strain at 0.1 s^{-1} at various temperatures for (**a**) Mn-Si and (**b**) Mo-Nb steel.

As far as the flow stress levels of the steels are concerned, it seems that there were no significant differences among the four steels tested, except the Mo-Nb steel (Figure 3b), which showed somewhat higher flow stresses especially at the two lowest deformation temperatures. As regards the Mn-Si steel, the maximum flow stress at 0.2 strain is comparable with the previous measurements made at the authors' laboratory for Mn-Si steels [25]. Grajcar et al. [30,39] reported that Mn did not affect the hot flow stress behaviour of 3%Mn and 5%Mn steels in the range 850–1150 °C. For better clarification of the effect of alloying elements on the flow stress level at low and high temperatures, flow stress curves of all four steels at two respective temperatures of 950 °C and 1150 °C, are plotted in Figure 4. Obviously, all three Nb-microalloyed steels exhibit slightly higher flow stresses at 950 °C (maximum stress 100–110 MPa at ~0.2 strain) in comparison to that of Mn-Si steel (90 MPa at ~0.2 strain), whereas at 1150 °C the effect of Nb-microalloying is not evident. Furthermore, the Mo-Nb steel has the highest flow stress at 950 °C (110 MPa at ~0.2 strain). In agreement, Singh et al. [40] reported increased flow stress in the range of 850–1100 °C, caused by solute drag and pinning effects in Mo- and Nb-alloyed low carbon steels. Kaikkonen et al. [5] also observed a noticeable increase in the mean flow stress at 900 °C in a Mo-Nb-alloyed medium-carbon steel.

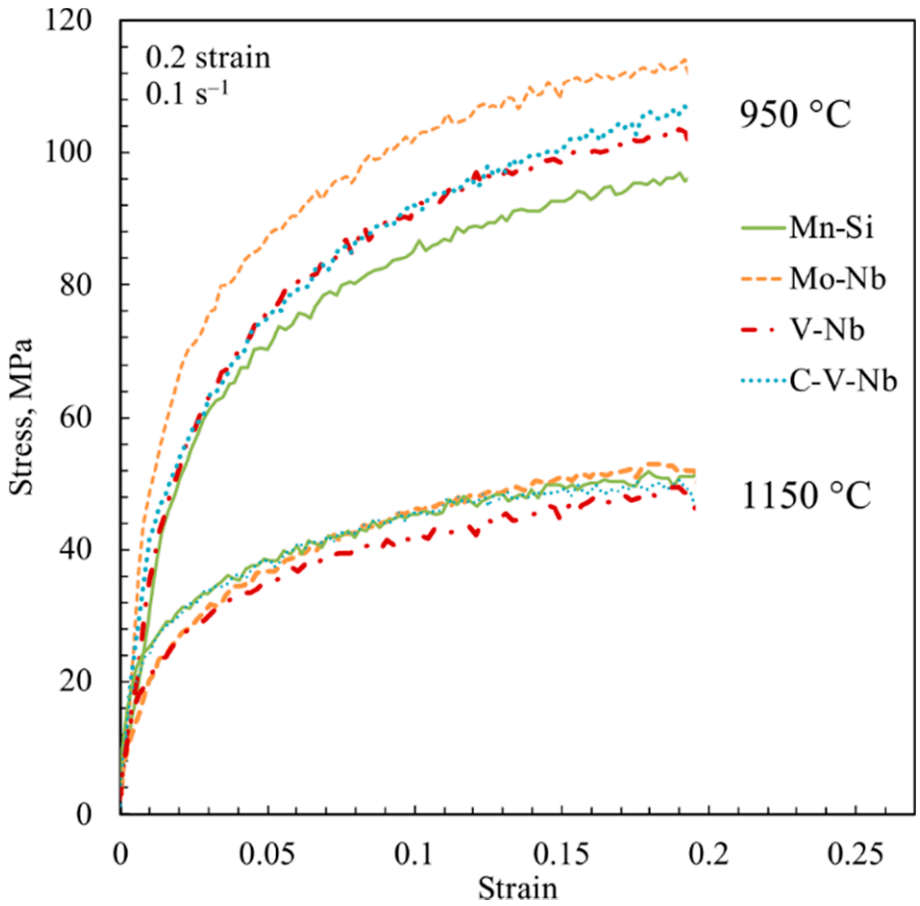

Figure 4. True stress–strain curves of the four steels at 1150 and 950 °C.

3.2. Stress Relaxation Behaviour

Typical stress-relaxation curves for the studied steels are plotted in Figure 5. Although the curves look somewhat flat at short relaxation times (note the logarithmic time scale) because of several curves plotted together, but the essential information, i.e., the three stages of the restoration process can still be discerned. Several earlier studies have presented that the initial and final linear stages of the curves correspond to the occurrence of static recovery and slow creep, respectively, and the intermediate faster drop in the stress level indicates the occurrence of either SRX or MDRX process, cf. [16,17,41]. Stress relaxation curves were carefully analysed to determine the characteristics of the SRX process as a function of deformation parameters. Recrystallized fraction vs. time curves stating the SRX (or MDRX) rates can be computed from the stress relaxation data by determining the slopes of the first and third stages [17,42].

An example of a stress relaxation curve fitted with the help of two lines (A and B) and determination of the recrystallized fraction X at a particular time is shown in Figure 6, as explained in [17,42]. More details and analysis of the experimental parameters on the SRX kinetics are discussed in subsequent sections.

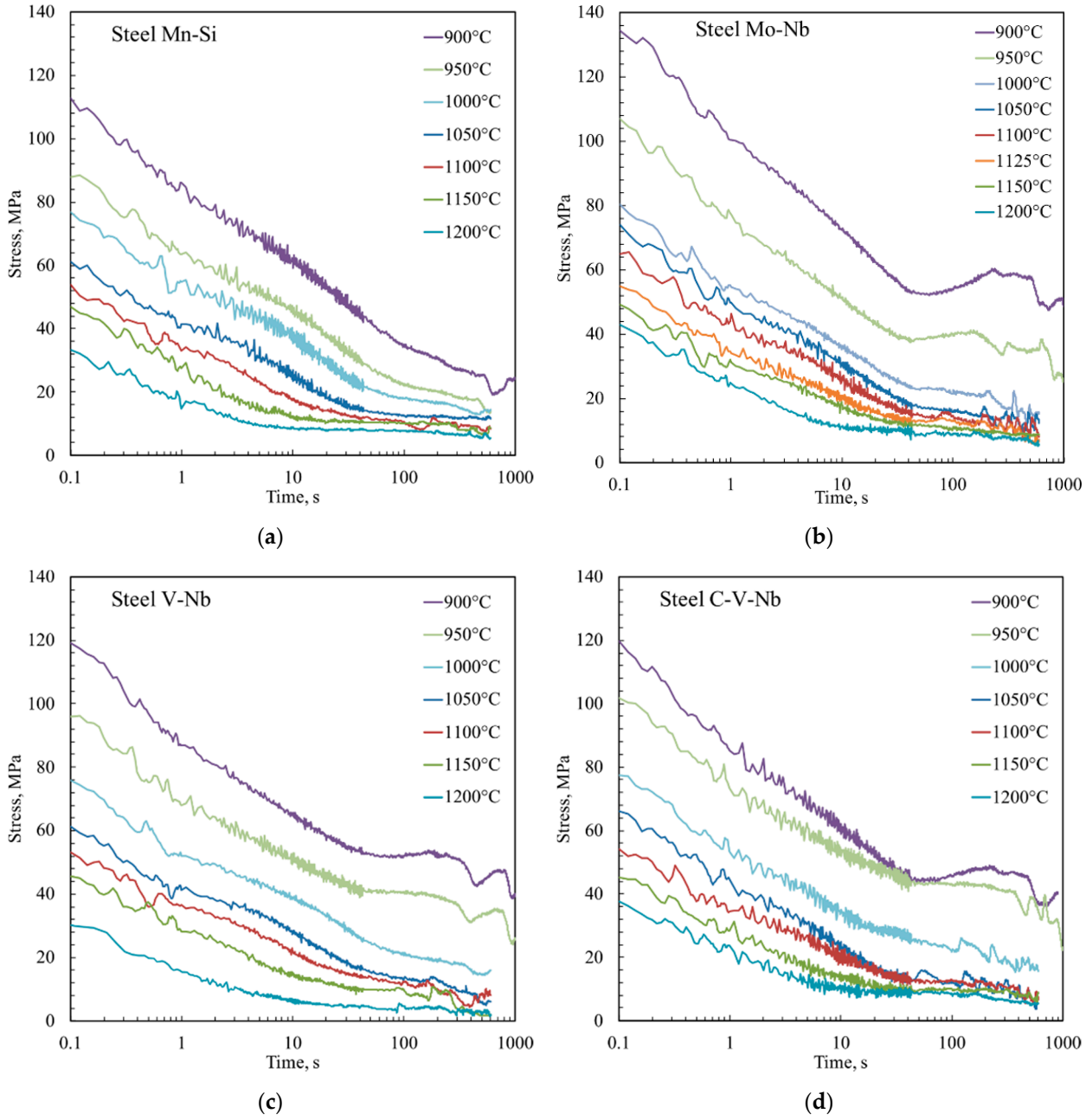

Figure 5. Typical stress relaxation curves obtained on the bainitic steels reheated at 1250 °C/2 min and compressed in the range 900–1200 °C to 0.2 strain at 0.1 s^{-1} for (**a**) Mn-Si, (**b**) Mo-Nb (**c**) V-Nb and (**d**) C-V-Nb.

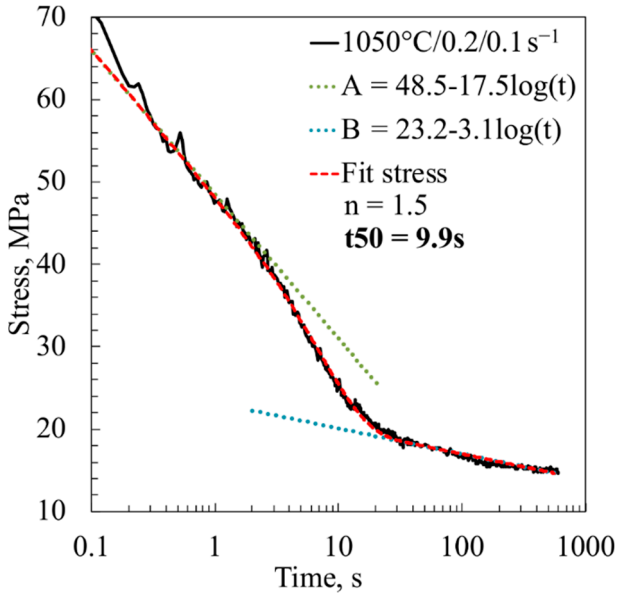

Figure 6. An example of fitting a stress relaxation curve (Mn-Si steel; reheating at 1250 °C/1 min, deformation at 1050 °C/0.2/0.1 s^{-1}) using the linear log-t slopes (A and B) for the stress in the 1st and 3rd stages for determining t_{50} and the Avrami exponent *n*.

3.3. Effect of Temperature and Precipitation on SRX Rate

From the stress relaxation data (Figure 5) and Equation (1) the SRX fraction X vs log-t data can be obtained, and examples are plotted in Figure 7. As shown in [16–18], the Avrami-type equation describing the SRX kinetics can be reasonably fitted with the data, as also demonstrated in the figure. From these curves, for instance, t_{50} times at different temperatures can be extracted. It is seen that the SRX rate increases significantly with an increase in the temperature from 900 °C to 1150 °C. For instance, in the case of Mn-Si steel, t_{50} decreases from 31 s at 1000 °C to 3 s at 1150 °C (Figure 7a). Complete softening was obtained in all studied cases, except at the lowest temperature of 900 °C, where the stress at the final stage remained clearly higher than seen at other temperatures, indicating that the recrystallization was only partial (see Figures 5a and 7a). Karjalainen [16] earlier demonstrated that in the instance of partial recrystallization, the stress relaxation curve remains at a relatively high stress level for the given temperature, although it still keeps declining.

As regards the Mo-Nb steel, the effect of temperature on the SRX kinetics is more complicated, as seen in Figure 5b. For instance, the time t_{50} increases from 3.5 s at 1175 °C to 30 s at 1075 °C. However, it can be noticed that the stress remained relatively high at the three lowest temperatures, 1000, 950 and 900 °C, denoting that the softening was incomplete. Furthermore, at 950 and 900 °C, the stress relaxation curves displayed plateaus (constant stress periods), or even a slight increase in the stress level after about 30–40 s, followed by a drop after about 300–400 s. It is well known that strain-induced precipitation results in an increase in stress level during stress relaxation manifesting as plateaus in the curves or even an increase in stress [6,9,11,26–28].

Similarly, for the V-Nb steel, SRX fraction data in Figure 7c show an enhanced SRX rate with an increase in the temperature. For instance, the t_{50} decreases from 49 s at 1000 °C to 1.6 s at 1200 °C. Obviously, the precipitation at 1000 °C and below, especially at 950 °C and 900 °C, seems to significantly affect the relaxation stress (see Figures 5c and 7c). Furthermore, at 950 and 900 °C, the precipitation halts are evident after about 30–40 s of relaxation. Thus, the appearance of plateaus through stress enhancement can be connected with the occurrence of carbide or carbonitride precipitation, as they were observed in all three Nb-bearing steels. A further decrease in stress could be due to coarsening of precipitates [27]. The start and finishing (coarsening) times of precipitation, Ps and Pf,

respectively, were determined from the stress relaxation curves and listed in Table 3, where some relevant data from literature are also included for comparison [6,26–29]. As seen, the range of precipitation temperatures and times in the current study correlated well with the data published in the literature.

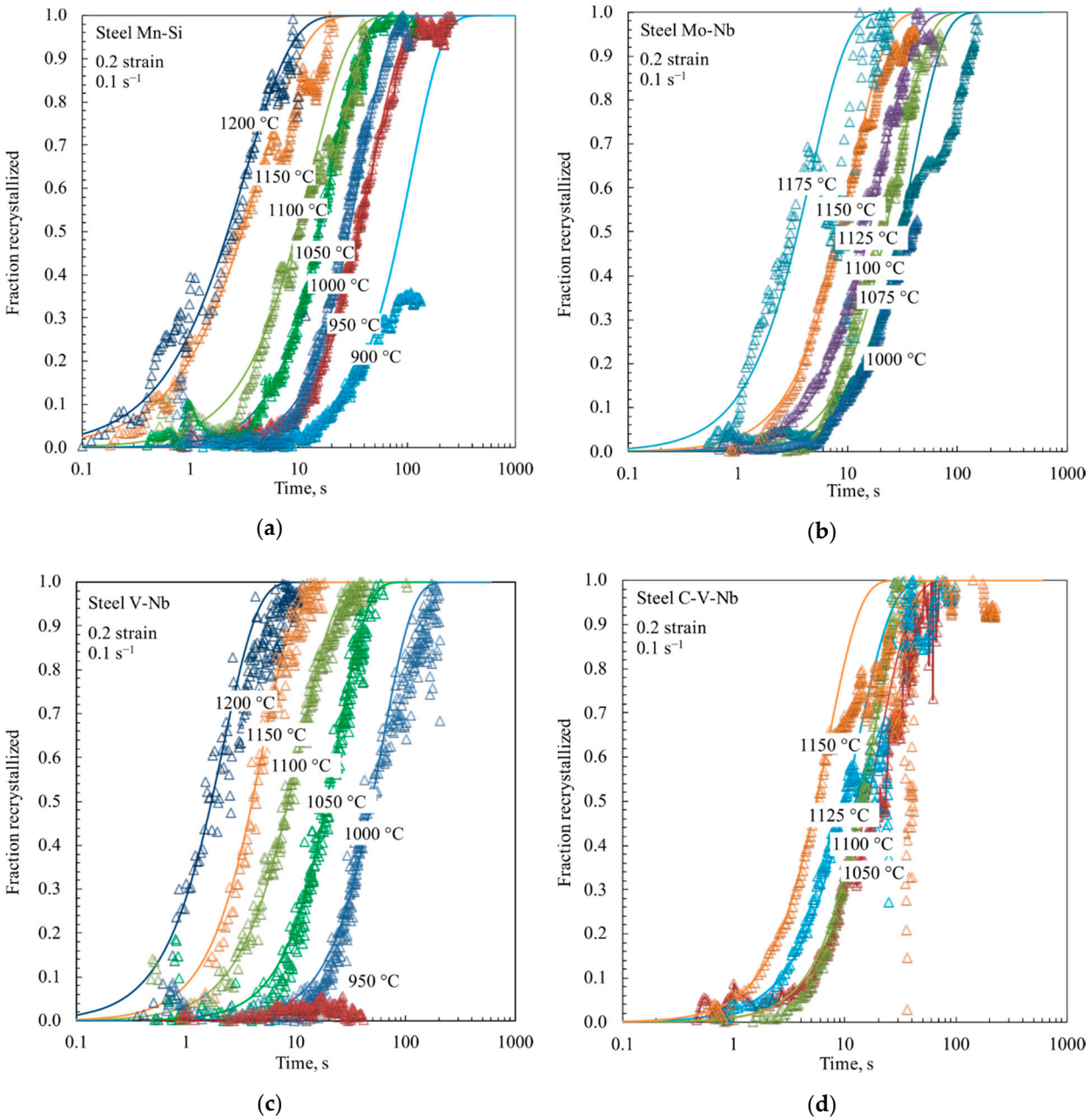

Figure 7. Fraction recrystallized vs. time data fitted with JMAK-type curves for (**a**) Mn-Si, (**b**) Mo-Nb, (**c**) V-Nb and (**d**) C-V-Nb.

The Avrami exponent was found to vary in a narrow range of 1.4–1.5, which is consistent with the typical exponents for low carbon steels [25].

Hot rolling is intended to take place in the recrystallization range, above T_{nr} temperature. The well-known Boratto equation [34] has been proposed for estimating T_{nr}, but as listed in Table 4, it does not give realistic values for the present steels having high Si content, and it does not include the effect of Mo. Thus, a modification for the Boratto equation is proposed based on the recrystallization behaviour of the present steels as Equation (3):

$$T_{nr} = 887 + 464C + (6445Nb - 644\sqrt{Nb}) + 500V + 363Al - 357Si + (400Mo - 175\sqrt{Mo}) \quad (3)$$

where the effect of V is changed (originally 732V–230$\sqrt{V}$) and the effect of Mo is added. C and Si are limited to the maximum of 0.4%. As seen from Table 4, the predicted values by the modified equation suggest T_{nr} values which are close to the approximate values which can be drawn from the relaxation curves (the lowest temperature resulting in complete recrystallization, Figures 5 and 7).

Table 3. Start and coarsening times of precipitation reported in the literature and obtained from the present relaxation tests.

Steel	Source	T_P [°C]	P_s [s]	P_f [s]
0.07C-0.96Mn-0.21Si-0.004V-0.046Nb-0.011Ti	Perttula [26]	900	30–50	
0.21C-1.1Mn-0.2Si-0.062V	Medina [27]	800–900	20–80	100–500
0.2C-1.0Mn-0.2Si-0.007Nb	Medina [27]	850–950	30–90	110–600
0.19C-1.5Mn-0.45Si-0.125V-0.035Nb	Pandit [6]	1000	30	100
0.11C-1.23Mn-0.23Si-0.048V-0.058Nb-0.017Ti	Buhler [29]	920	25	550
0.06C-1.9Mn-0.33Si-0.09Nb-0.01Ti	Lan [28]	900–1000	7–30	10–50
Mo-Nb	Current study	900–950	30–40	300–400
V-Nb	Current study	900–950	30–40	150–500

Table 4. T_{nr} temperatures as estimated by the Boratto equation, calculated by the modified Boratto equation and approximated from stress relaxation data.

Steel Code	Boratto T_{nr} (°C)	Regression T_{nr} (°C)	Approx. T_{nr} (°C)
Mn-Si	596	901	900
Mo-Nb	674	1018	1015
V-Nb	645	999	1000
C-V-Nb	697	1014	1020

3.4. Powers of Strain and Strain Rate

The powers of strain (p) and strain rate (q) in Equation (1) were estimated by plotting (i) t_{50} versus strain between 0.125–0.4 at 0.1 s^{-1} at a particular temperature, 1050 °C or 1100 °C, and (ii) t_{50} versus the strain rate between 0.01–5 s^{-1}, following compression to 0.2 strain at 1050 °C. The corresponding plots for all four steels are displayed in Figure 8. The powers p and q may be determined from the linear slopes of the data points in the log–log plot. Alternatively, a power function appears as a linear fit when plotted in a log–log plot. The power functions and their determination coefficients (R^2) are listed in Figure 8. Determination coefficients vary in the range of 0.89–0.99, which is a reasonable level when scatter in the data is expected.

The values of p in Figure 8a are −2.2, −2.7, −1.9 and −1.7 for steels Mn-Si, Mo-Nb, V-Nb and C-V-Nb, respectively. They are rather low, as the typical values reported in the literature vary between −4 and −2 [18,21–23,25,33,43,44], and for microalloyed steels between −3 and −2 [18,26,41]. Values of −2.8 and −2.5 for the strain exponent p were estimated by Somani et al. [15,16,19] for C/C–Mn/Nb/Ti/Nb–Ti and Mn–V steels, respectively [18,23,25]. Lang et al. [45] and Suikkanen et al. [24] obtained −2.1 for p in the case of a 0.2C-2.0Mn-1.48Si-0.6Cr steel, which is very close to the Mn-Si steel used in the present study (0.4C-2.0Mn-1.3Si-0.7Cr; Table 1) except for the difference in C content. The present steels contain 0.7% Cr, but the low concentrations of Cr have hardly shown any influence on the SRX kinetics of C-Mn steels [39,46,47] and therefore Cr cannot be expected to have any significant influence on the power of strain or strain rate.

It was observed that all experimental values of the strain rate exponent q fall within a rather narrow range (−0.21, −0.26, −0.28, −0.27 for Mn-Si, Mo-Nb, V-Nb and C-V-Nb, respectively), indicating a weak dependence of SRX on the strain rate, irrespective of the steel alloying. Lang et al. [46] and Suikkanen et al. [24] determined the power of the strain rate q to be −0.18 for a 0.2C-2.0Mn-1.48Si-0.6Cr steel. This value of q is slightly lower than the value −0.21 obtained for the present Mn-Si steel, although there is a significant scatter in the data (see Figure 8a). For Nb and Nb–Ti and also Mo-steels, q has been reported to be

approximately −0.26, which is in good agreement with the q obtained for the microalloyed steels in the current study (−0.26, −0.28, −0.27) [18,23].

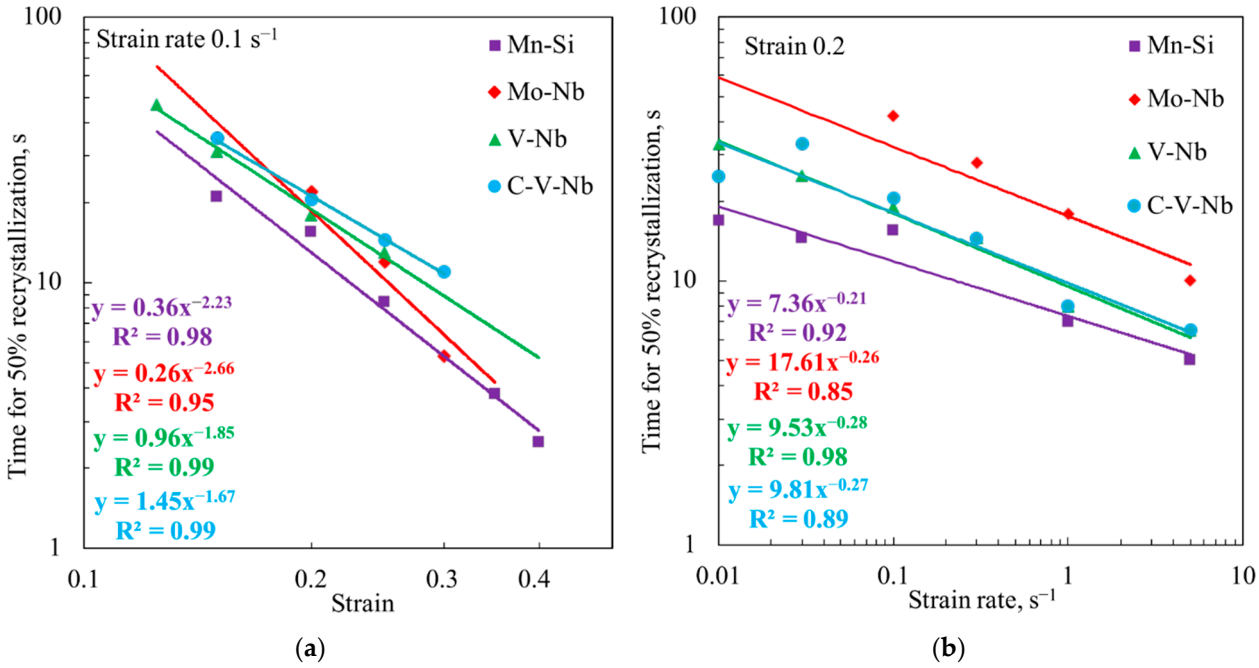

Figure 8. Dependence of t_{50} on (**a**) strain and (**b**) the strain rate for experimental steels deformed at 1050 °C, except Mo-Nb, which is deformed and relaxed at 1100 °C. See Table 1 for austenite grain size of the steels.

3.5. Effect of Grain Size on SRX Rate

To understand the effect of grain size on the SRX rate, different reheating temperatures and/or times were selected to vary the grain size. For instance, Mn-Si steel specimens reheated at 1250 °C for 2 min resulted in a very coarse grain size of ~650 µm, whereas holding for just 1 min at the same temperature resulted in a grain size of 132 µm. The stress relaxation data (1050 °C/0.2/0.1 s^{-1}) revealed t_{50} times of 15.5 s and 9.9 s (see Figure 9a) for the two grain sizes, respectively, i.e., a significant retardation of SRX rate by grain coarsening in the instance of very coarse grain size. Similarly, reheating Mo-Nb steel at 1250 °C/2 min resulted in a grain size of 461 µm in comparison to 157 µm obtained at 1150 °C/2 min. The corresponding t_{50} times were 30.0 s and 16.6 s (see Figure 9b), respectively. More details about the grain size data for the experimental steels corresponding to different reheating temperatures and/or times are given in Table 2. Similar effects of grain size on the SRX rate were observed in other steels, as well. These were later used in validation of empirical equations developed in this study and also compared with the predictions of the previous model for microalloyed steels [18,21–23].

3.6. Apparent Activation Energy of Recrystallization (Q_{app})

For estimating the apparent activation energy for recrystallization (Q_{app}), the t_{50} data, as expressed in Equation (1), was plotted against the inverse absolute temperature (1/T) in Figure 10, where the corresponding R^2 values are also presented. In the analysis of the t_{50} data, the cases of incomplete recrystallization (at low temperatures) and MDRX (at high temperatures) were systematically excluded. The possibility of partial recrystallization at low temperatures were discussed earlier (see Section 3.3), whereas the occurrence of MDRX was suspected at high temperatures 1150–1200 °C as well as at high strains 0.35–0.4 for the three Nb microalloyed steels. From the plots, the Q_{app} was estimated as 225, 268, 260 and 269 kJ·mol^{-1} for Mn-Si, Mo-Nb, V-Nb and C-V-Nb steels, respectively. For comparison, t_{50} data for a 0.3-2Mn-1.5Si steel from Somani et al. [25] were also included in the figure.

Despite the different carbon contents of 0.3%C and 0.4%C of the two Mn-Si steels, the Q_{app} of 224.6 kJ/mol was the same as that of the current Mn-Si steel (225 kJ/mol). However, the measured t_{50} times for the 0.3C-2Mn-1Si were significantly shorter than for the current Mn-Si steel, obviously as a consequence of its finer austenite grain size (132 µm vs. 650 µm), and not due to the different carbon content.

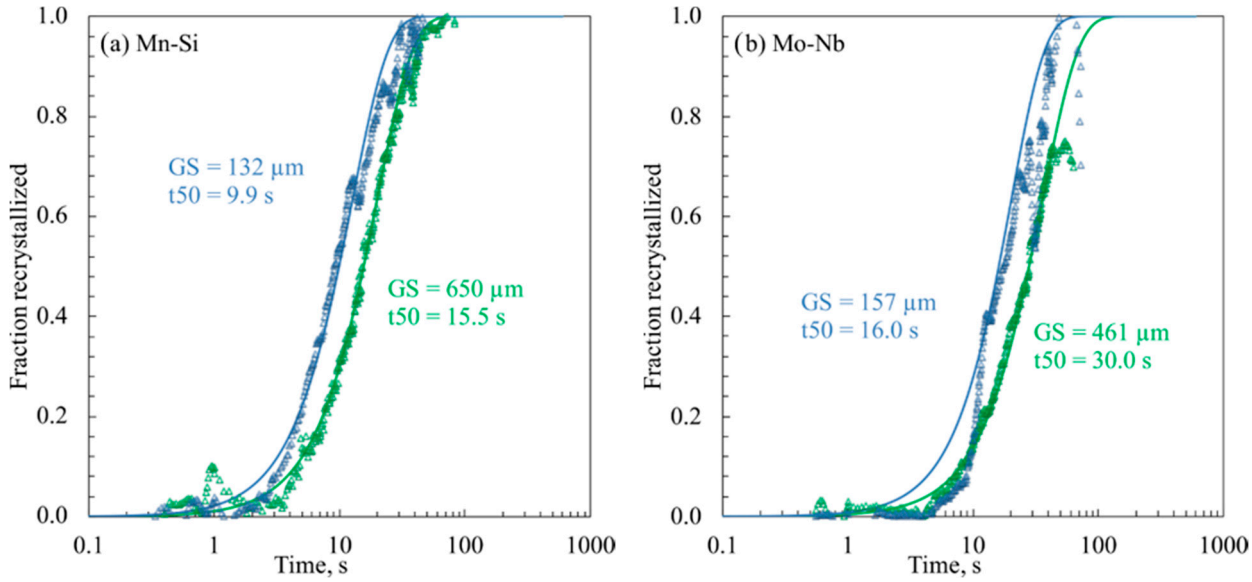

Figure 9. Recrystallized fraction vs. time (1050 °C/0.2/0.1 s^{-1}) curves after two austenitization conditions revealing the effect of grain size: (**a**) Mn-Si at 1250 °C for 1 and 2 min and (**b**) Mo-Nb, at 1150 and 1250 °C for 2 min.

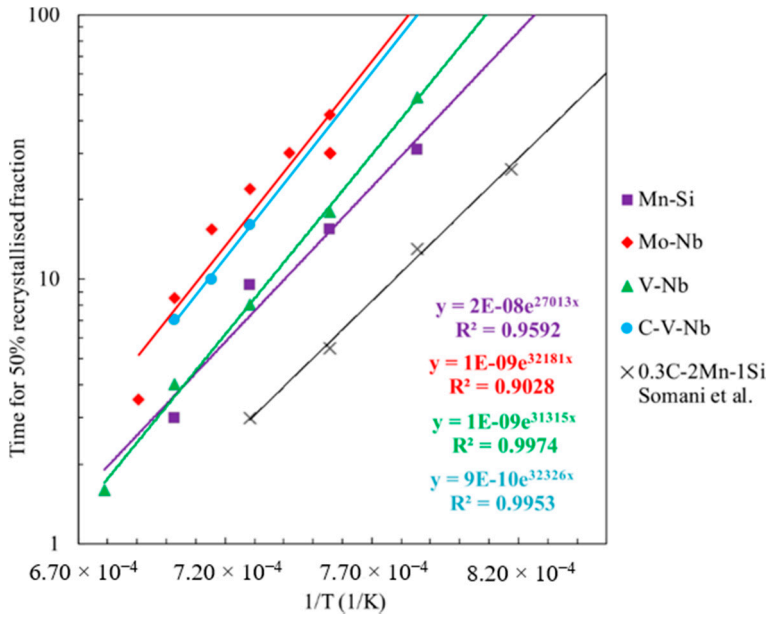

Figure 10. Estimation of Q_{app} of the experimental steels. Data of 0.3C-2Mn-1Si steel are also included for comparison [25].

3.7. Effect of Mo, V and Nb on Q_{rex}

The activation energy of SRX (Q_{rex}) is dependent on the Q_{app}, the power of strain rate q, and the activation energy of deformation Q_{def}. Somani et al. [18,21,22,25] considered the Q_{def} of 340 kJ/mol for C–Mn steels and 400 kJ/mol for Nb-microalloyed steels while developing the regression model for the Q_{rex} of hot deformed austenite. Suikkanen et al. [32] reported

Q_{def} values increasing in the range 324 to 353 kJ/mol for 0.2C-2.0Mn-0.6Cr-Si steels with the Si content increasing from 0.04% to 1.48%. Cabañas et al. [48] determined the effect of Mn on Q_{def} in Fe-Mn binary systems and reported that generally Mn, below 10%, increased the Q_{def} whereas Mn contents ≥10% decreased it, although the maximum Q_{def} was obtained for an Fe-3Mn alloy.

If assuming that the Q_{def} is 340 kJ/mol for Mn-Si steel, Q_{rex} of 296 kJ/mol is obtained, and considering a Q_{def} of 400 kJ/mol for the current Nb-microalloyed steels would result in Q_{rex} values of 372, 372 and 377 kJ/mol for Mo-Nb, V-Nb and C-V-Nb steels, respectively. It can be noted that the value of q for Mn-Si steel (−0.21) was somewhat lower than those of Mo-Nb (−0.26), V-Nb (−0.28) and C-V-Nb (−0.27) steels, so that the relatively low Q_{app} value (225 kJ/mol) of Mn-Si steel results in a lower Q_{rex} value than in the other steels, as also expected from its lower alloying content. Nevertheless, the Q_{rex} values of Mo-Nb and V-Nb steels was equal (372 kJ/mol). The only difference between the V-Nb and C-V-Nb steel is the carbon content (see Table 1). The difference 0.4% and 0.5% in the carbon content cannot be expected to cause any difference, so the slightly different values of p, q, Q_{app} and Q_{rex} can be attributed to simple data scatter.

A linear regression analysis [18,21,22] suggested that Q_{rex} (in J/mol) for C–Mn and microalloyed steels can be given by:

$$Q_{\text{rex}} = 3803\text{CF} + 109{,}418 \quad (4)$$

Here *CF*, the composition factor, is:

$$\text{CF} = 2\text{Cr} + 10\text{Cu} + 15\text{Mn} + 50\text{Mo} + 60\text{Si} + 70\text{V} + 230\text{Ti} + 700\text{Nb} \quad (5)$$

where the elements are in wt.% and the effects of Si and Nb are considered to saturate at 0.4% and 0.044%, respectively. These equations lead to Q_{rex} values of 323, 445, 400, and 401 kJ/mol, respectively for the Mn-Si, Mo-Nb, V-Nb and C-V-Nb steels. The predicted value of 323 kJ/mol for the Mn-Si is slightly higher than the experimentally obtained value (296 kJ/mol), whereas for the Nb-microalloyed steels the predicted values are remarkably higher than the experimental ones. As the predictions of Q_{rex} deviate for all four steels in the same direction, it might suggest that the regression is not valid with 2%Mn, but the upper limit of saturation should be lower, or the coefficient of Mn should be lower. Decreasing the coefficient of Mn in the Equation (5) from 15 to 11 could result in more comparable Q_{rex} values, specifically 293, 415, 370 and 372 kJ/mol for the Mn-Si, Mo-Nb, V-Nb and C-V-Nb steels, respectively. However, the difference in the predicted and obtained value still remains notably high for the Mo-Nb steel (372 kJ/mol and 415 kJ/mol).

3.8. Fractional Softening Equations

In Equation (1), the power of the grain size (s) described by the relation $s = 2.13d^{-0.105}$ was previously determined based on measured SRX data for a large number of carbon steels, with and without microalloying [18]. The constant A for the present four experimental steels could be obtained by taking s by the same relation, together with the values for the other parameters (Q_{app}, p and q) in Equation (1). Finally, t_{50} can be described by the following SRX equations:

$$\text{Mn-Si} \qquad t_{50} = 2.63 \times 10^{-13}\ \varepsilon^{-2.2}\ \varepsilon'^{-0.21}\ d^{s}\ \exp(225{,}000/RT) \quad (6)$$

$$\text{Mo-Nb} \qquad t_{50} = 8.66 \times 10^{-15}\ \varepsilon^{-2.7}\ \varepsilon'^{-0.26}\ d^{s}\ \exp(268{,}000/RT) \quad (7)$$

$$\text{V-Nb} \qquad t_{50} = 2.71 \times 10^{-14}\ \varepsilon^{-1.9}\ \varepsilon'^{-0.28}\ d^{s}\ \exp(260{,}000/RT) \quad (8)$$

$$\text{C-V-Nb} \qquad t_{50} = 2.11 \times 10^{-14}\ \varepsilon^{-1.7}\ \varepsilon'^{-0.27}\ d^{s}\ \exp(269{,}000/RT) \quad (9)$$

The predictions for all four steels including confirmation tests for Mn-Si steel and a comparison with the predictions of an equation for V-Nb steel from Shen et al. [49] are

displayed in Figure 11. A reasonable consistence is obvious, although the experimental scatter is pronounced.

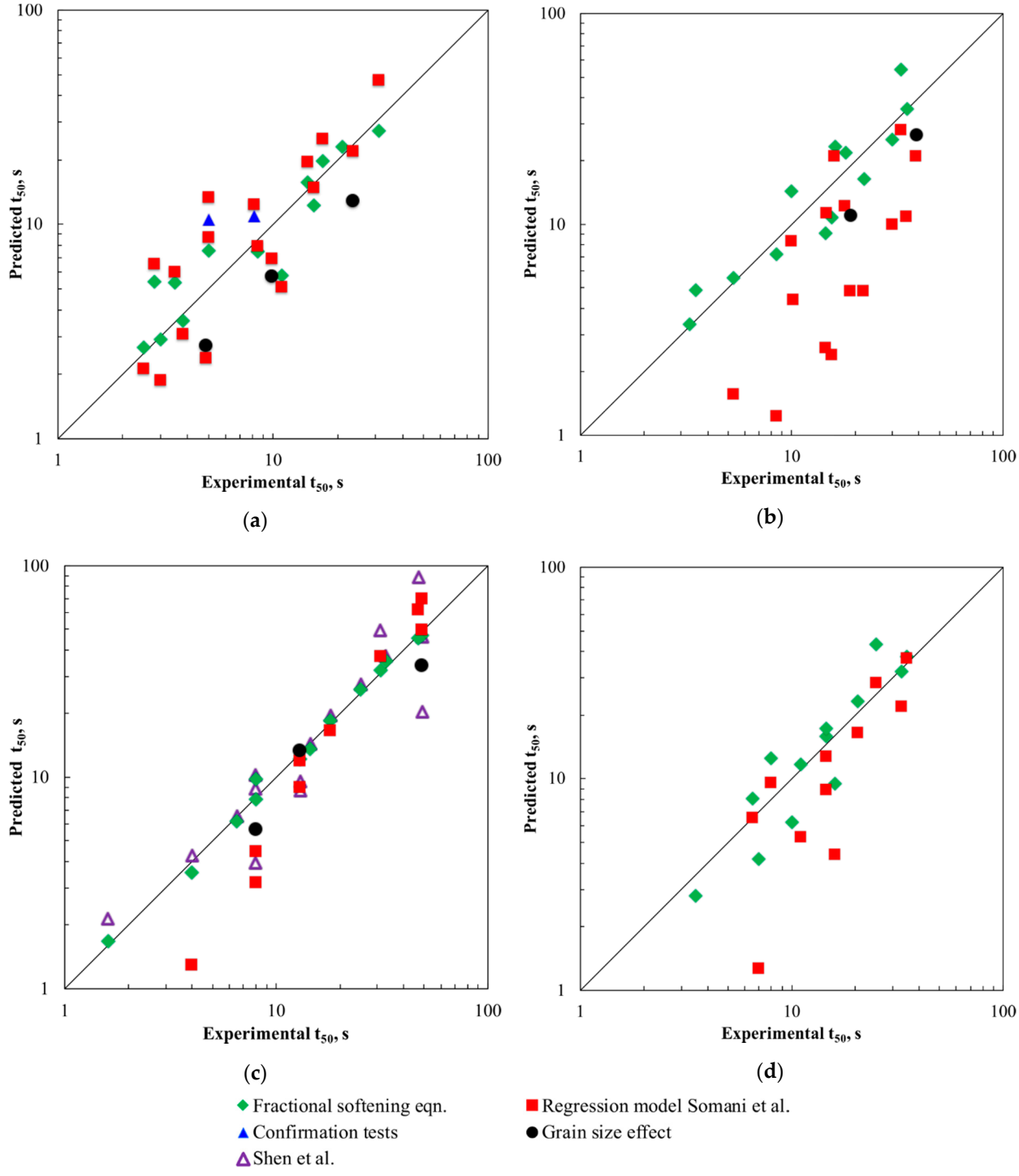

Figure 11. Predictions vs. experimental t_{50} times: (**a**) Mn-Si, (**b**) Mo-Nb, (**c**) V-Nb and (**d**) C-V-Nb steels. Confirmation tests for Mn-Si steel, predicted data of Shen et al. [49] for a V-Nb steel and the predictions of previous regression model [21–23] experimental data for different grain sizes are also included for comparison. The only test for grain size effect in the case of C-V-Nb steel was not successful.

In order to check the reliability of the fractional softening Equation (9) derived for the Mn-Si steel, two confirmation experiments were conducted by randomly varying the deformation parameters, (1075 °C/0.17/0.15 s^{-1}, 1025 °C/0.24/0.2 s^{-1}) and using

a coarse grain size (650 μm; see Table 1). As seen in Figure 11, the predictions for the confirmation tests resulted in reasonable predicted/experimental ratios of 1.3 and 2.0, for 1025 °C/0.24/0.2 s^{-1} and 1075 °C/0.17/0.15 s^{-1} respectively.

The results of the prior regression model developed for estimating t_{50} [18,21–23] are also shown in Figure 11. It is obvious that the previous model generally predicts shorter t_{50} times than the present model and experimental values obtained for the microalloyed steels, whereas for the Mn-Si steel those predictions follow more closely the agreement line, although with large scatter. From Figure 11, it can be seen that the predicted values deviated from experimental ones particularly for the Mo-Nb steel and to some extent for C-V-Nb steel. Two reasons may be suggested for this deviation: first the pronounced scatter of the data (after many repeats) and secondly because of the unsuitability of the prior model for very coarse grain sizes (450–650 μm) existing in the present experiments. The predicted/experimental ratios using the empirical equations derived in this study are in range of 0.6–2 for Mn-Si, 0.6–2.1 for Mo-Nb, 0.7–1.2 for V-Nb and 0.6–4.0 for C-V-Nb steels, where the grain size variation results in some scatter. Grain size effect is determined from data from different reheating temperatures or times (see Table 2).

4. Conclusions

The stress relaxation method on a Gleeble simulator was used to determine the static recrystallization (SRX) kinetics of coarse-grained hot-deformed austenite in four medium-carbon Fe-2Mn-1.3Si-0.7Cr steels with different microalloying over a wide range of temperatures (900–1200 °C), strains (0.125–0.4) and strain rates (0.01–5 s^{-1}). The effects of Mo and V together with Nb on SRX kinetics and the plausible occurrence of precipitation were thoroughly investigated. The main results are as follows:

Strain hardening and dynamic recovery occurred during compression under all deformation conditions. At low (≈950 °C) temperatures, V-Nb microalloying and particularly Mo-Nb alloying increased the flow stress.

The stress relaxation method was capable to reveal the SRX kinetics under various conditions and new Avrami-type equations could be established based on the recorded relaxation data.

V-Nb microalloying and particularly the Mo-Nb alloying retarded the SRX kinetics, whereas the difference between carbon contents of 0.4% and 0.5% (both with Nb microalloying) was considered minor and attributed to data scatter. For instance, the t_{50} times are 9.9, 30.0, 18.0 and 20.5 s for Mn-Si, Mo-Nb, V-Nb and C-V-Nb, respectively, at 1050 °C (strain 0.2, strain rate 0.1 s^{-1}, though it should be emphasized that grain sizes vary among the steels).

In the Avrami-type equation, the powers of strain p (−1.7 to −2.7) and strain rate q (−0.21 to −0.28) were in the same range as reported earlier for C-Mn microalloyed steels. Thus, the influence of V and Mo in connection with Nb is negligible.

The apparent activation energy of SRX increased due to V-Nb and Mo-Nb alloying (260–269 kJ/mol) but the Q_{app} of the Mn-Si steel (225 kJ/mol) without microalloying was in the range reported earlier for C-Mn microalloyed steels with lower Mn and Si contents.

The prior SRX regression model suggested for hot deformed austenite [21–23] showed reasonable 50% recrystallization times (t_{50}) for the Mn-Si steel, but for the present microalloyed steels the predicted values were distinctly shorter than the experimental ones. A very large grain size of the present steels might be a reason for the discrepancy.

Stress relaxation curves also revealed the occurrence of partial recrystallization and the start of precipitation at low deformation temperatures. Strain-induced precipitation occurred after 30–40 s at around 950 °C for V- and Mo-Nb steels.

The Boratto equation for predicting the T_{nr} temperature was modified successfully for these medium carbon bainitic steels containing high silicon, whereby the effect of V was changed, and C and Si were limited to the maximum of 0.4%, in order to include the influence of Mo alloying.

The equations derived to describe the SRX kinetics can be used in the design of the industrial rough rolling scheme of thermomechanical processing to avoid partial recrystallization.

Author Contributions: Conceptualization, M.C.S. and L.P.K.; formal analysis, P.M.K. and M.C.S.; data curation, P.M.K.; writing—original draft preparation, P.M.K.; writing—review and editing, M.C.S. and L.P.K.; visualization, P.M.K.; supervision, J.I.K.; project administration; J.I.K. All authors have read and agreed to the published version of the manuscript.

Funding: This research was funded by European Research Fund for Coal and Steel under the contract RFCS-2015-709607 and the Academy of Finland under the "Genome of Steel" project #311934.

Institutional Review Board Statement: Not applicable.

Informed Consent Statement: Not applicable.

Data Availability Statement: The raw/processed data required to reproduce these findings cannot be shared at this time as the data also forms part of an ongoing study.

Acknowledgments: The authors would like to thank Juha Uusitalo for conducting the stress-relaxation experiments on the Gleeble simulator.

Conflicts of Interest: The authors declare no conflict of interest.

References

1. Sourmail, T.; Smanio, V.; Ziegler, C.; Heuer, V.; Kuntz, M.; Caballero, F.G.; Garcia-Mateo, C.; Cornide, J.; Elvira, R.; Leiro, A.; et al. Novel nanostructured bainitic steel grades to answer the need for high-performance steel components (Nanobain). *RFSR* **2013**. [CrossRef]
2. Garcia-Mateo, C.; Paul, G.; Somani, M.; Porter, D.; Bracke, L.; Latz, A.; de Andres, C.G.; Caballero, F.G. Transferring nanoscale bainite concept to lower C contents: A perspective. *Metals* **2017**, *7*, 159. [CrossRef]
3. Fan, H.L.; Zhao, A.M.; Li, Q.C.; Guo, H.; He, J.G. Effects of ausforming strain on bainite transformation in nanostructured bainite steel. *Int. J. Miner. Metall. Mater.* **2017**, *24*, 264–270. [CrossRef]
4. Zhang, M.; Wang, Y.H.; Zheng, C.L.; Zhang, F.C.; Wang, T.S. Effects of ausforming on isothermal bainite transformation behaviour and microstructural refinement in medium-carbon Si-Al-rich alloy steel. *Mater. Des.* **2014**, *62*, 168–174. [CrossRef]
5. Kaikkonen, P.M.; Somani, M.C.; Miettunen, I.H.; Porter, D.A. Constitutive flow behaviour of austenite at low temperatures and its influence on bainite transformation characteristics of ausformed. *Mater. Sci. Eng.* **2020**, *775*, 9–11. [CrossRef]
6. Pandit, A.; Murugaiyan, A.; Podder, A.S.; Haldar, A.; Bhattacharjee, D.; Chandra, S.; Ray, R.K. Strain induced precipitation of complex carbonitrides in Nb-V and Ti-V microalloyed steels. *Scr. Mater.* **2005**, *53*, 1309–1314. [CrossRef]
7. Medina, S.F.; Mancilla, J.E. Static recrystallization modelling of hot deformed steels containing several alloying elements. *ISIJ Int.* **1996**, *36*, 1070–1076. [CrossRef]
8. García-Mateo, C.; López, B.; Rodriguez-Ibabe, J.M. Static recrystallization kinetics in warm worked vanadium microalloyed steels. *Mater. Sci. Eng. A* **2001**, *303*, 216–225. [CrossRef]
9. Vervynckt, S.; Verbeken, K.; Thibaux, P.; Liebeherr, M.; Houbaert, Y. Control of the austenite recrystallization in niobium microalloyed steels. *Mater. Sci. Forum* **2010**, *638–642*, 3567–3572. [CrossRef]
10. Esterl, R.; Sonnleitner, M.; Schnitzer, R. Microstructural analysis of the recrystallization behavior of low alloyed steels. *Steel Res. Int.* **2019**, *90*, 1–10. [CrossRef]
11. Pereda, B.; López, B.; Rodriguez-Ibabe, J.M. Increasing the non-recrystallization temperature of Nb microalloyed steels by Mo addition. In Proceedings of the Microstructure, Properties and Performance Proceedings, Pittsburgh, PA, USA, 1–3 July 2007; pp. 151–159.
12. Liu, W.J.; Jonas, J.J. A stress relaxation method for following carbonitride precipitation in austenite at hot working temperatures. *Metall. Trans. A* **1988**, *19*, 1403–1413. [CrossRef]
13. Medina, S.F.; Quispe, A. Improved model for static recrystallization kinetics of hot deformed austenite in low alloy and Nb/V microalloyed steels. *ISIJ Int.* **2001**, *41*, 774–781. [CrossRef]
14. Sellars, C.M.; Whiteman, J.A. Recrystallization and grain growth in hot rolling. *Met. Sci.* **1979**, *13*, 187–194. [CrossRef]
15. Sellars, C.M.; Davies, G.J. Hot working and forming processes. In Proceedings of the International Conference Organized Jointly by the Sheffield Metallurgical and Engineering Association and the University of Sheffield in Assocation with The Metals Society, London, UK, 8 January 1980.
16. Karjalainen, L.P. Stress relaxation method for investigation of softening kinetics in hot deformed steels. *Mater. Sci. Technol.* **1995**, *11*, 557–565. [CrossRef]
17. Karjalainen, L.P.; Perttula, J. Characteristics of static and metadynamic recrystallization and strain accumulation in hot-deformed austenite as revealed by the stress relaxation method. *ISIJ Int.* **1996**, *36*, 729–736. [CrossRef]

18. Somani, M.C.; Karjalainen, L.P.; Porter, D.A.; Morgridge, A.R. Regression modelling of the recrystallization kinetics of austenite. In *Thermomechanical Processing: Mechanics, Microstructure and Control*; The University of Sheffield, Dept. of Engineering Materials: Sheffield, UK, 2002; pp. 436–441.
19. Elwazri, A.M.; Essadiqi, E.; Yue, S. Kinetics of metadynamic recrystallization in microalloyed steels. *ISIJ Int.* **2004**, *44*, 744–752. [CrossRef]
20. Lin, Y.C.; Chen, M.S.; Zhong, J. Study of static recrystallization kinetics in a low alloy steel. *Comput. Mater. Sci.* **2008**, *44*, 316–321. [CrossRef]
21. Somani, M.C.; Karjalainen, L.P. Validation of the new regression model for the static recrystallisation of hot-deformed austenite in special steels. In *Materials Science Forum*; Trans Tech Publications Ltd.: Baech, Switzerland, 2004; pp. 335–340. [CrossRef]
22. Somani, M.C.; Karjalainen, L.P. Modelling the deformation and annealing processes: Physical and regression approaches. *Mater. Sci. Forum* **2007**, *550*, 583–588. [CrossRef]
23. Somani, M.C.; Karjalainen, L.P. A rationale for SRX regression model of hot-deformed austenite using an orthogonal Taguchi L8 matrix steels. In *Materials Science Forum*; Trans Tech Publications Ltd.: Baech, Switzerland, 2012; pp. 751–757. [CrossRef]
24. Suikkanen, P.P.; Lang, V.T.E.; Somani, M.C.; Porter, D.A.; Karjalainen, L.P. Effect of silicon and aluminium on austenite static recrystallization kinetics in high-strength TRIP-aided steels. *ISIJ Int.* **2012**, *52*, 471–476. [CrossRef]
25. Somani, M.C.; Porter, D.A.; Karjalainen, L.P.; Kantanen, P.K.; Kömi, J.I.; Misra, D.K. Static recrystallization characteristics and kinetics of high-silicon steels for direct quenching and partitioning. *Int. J. Mater. Res.* **2019**, *110*, 183–193. [CrossRef]
26. Perttula, J.; Kantanen, P.; Karjalainen, P. Effect of precipitation on flow stress and recrystallization in Nb- and Ti-bearing austenite. *Scand. J. Metall.* **1998**, *27*, 128–132.
27. Medina, S.F.; Quispe, A.; Gómez, M. Strain induced precipitation effect on austenite static recrystallisation in microalloyed steels. *Mater. Sci. Technol.* **2003**, *19*, 99–108. [CrossRef]
28. Lan, L.Y.; Qiu, C.L.; Zhao, D.W.; Gao, X.H.; Du, L.X. Dynamic and static recrystallization behavior of low carbon high niobium microalloyed steel. *J. Iron Steel Res. Int.* **2011**, *18*, 55–60. [CrossRef]
29. Buhler, M.; Gomez, G.R.; Pérez, T. Effect of Nb in solid solution on the austenite decomposition kinetic of a V-Nb-Ti microalloyed steel. In Proceedings of the 1st International Conference, Super-High Strength Steels, Rome, Italy, 2–4 November 2005; pp. 1–10.
30. Grajcar, A.; Kuziak, R. Softening kinetics in Nb-microalloyed TRIP steels with increased Mn content. In *Advanced Materials Research*; Trans Tech Publications Ltd.: Baech, Switzerland, 2011; pp. 119–122. [CrossRef]
31. Rees, G.I.; Perdrix, J.; Maurickx, T.; Bhadeshia, H. The effect of niobium in solid-solution on the transformation kinetics of bainite. *Mater. Sci. Eng.* **1995**, *194*, 179–186. [CrossRef]
32. Dutta, B.; Valdes, E.; Sellars, C.M. Mechanism and kinetics of strain induced precipitation of Nb(C,N) in austenite. *Acta Metall. Mater.* **1992**, *40*, 653–662. [CrossRef]
33. Lenard, J.G.; Pietrzyk, M.; Cser, L. *Mathematical and Physical Simulation of the Properties of Hot Rolled Products*; Elsevier Science Ltd.: Amsterdam, The Netherlands, 1999; ISBN 9780080427010. [CrossRef]
34. Barbosa, R.; Boratto, F.; Yue, S.; Jonas, J.J. The influence of chemical composition on the recrystallisation behaviour of microalloyed steels. In *Processing, Microstructure and Properties of HSLA Steels*; The Minerals, Metals & Materials Society (TMS): Warrendale, PA, USA, 1988; pp. 51–61.
35. Bai, D.; Bodnar, R.; Ward, J.; Dorricott, J.; Sande, S. Development of discrete X80 line pipe at SSAB Americas. In *International Symposium on the Recent Developments in Plate Steels*; The Association for Iron & Steel Technology (AIST): Warrendale, PA, USA, 2011; Available online: http://digital.library.aist.org/pages/PR-258-002.htm (accessed on 8 December 2020).
36. Rollett, A.; Humphreys, F.; Rohrer, G.S.; Hatherly, M. *Recrystallization and Related Annealing Phenomena*, 2nd ed.; Elsevier Ltd.: Amsterdam, The Netherlands, 2004. [CrossRef]
37. Avrami, M. Kinetics of phase change. II Transformation-time relations for random distribution of nuclei. *J. Chem. Phys.* **1940**, *8*, 212–224. [CrossRef]
38. Sakui, S.; Sakai, T.; Takeishi, K. Hot deformation of austenite in a plain carbon steel. *Trans. Iron. Steel Inst. Jpn.* **1977**, *17*, 718–725. [CrossRef]
39. Grajcar, A.; Kuziak, R. Dynamic recrystallization behavior and softening kinetics in 3Mn-1.5Al TRIP steels. In *Advanced Materials Research*; Trans Tech Publications Ltd.: Baech, Switzerland, 2011; pp. 330–333. [CrossRef]
40. Singh, N.; Kostryzhev, A.G.; Killmore, C.R.; Pereloma, E.V. Effect of Mo, Nb and V on hot deformation behaviour, microstructure and hardness of microalloyed steels. In *Materials Science Forum*; Trans Tech Publications Ltd.: Baech, Switzerland, 2018; pp. 3–8. [CrossRef]
41. Karjalainen, L.; Pettula, J.; Xu, Y.; Niu, J. Stress relaxation, a novel technique for measuring the softening kinetics in hot-deformed austenite. In Proceedings of the 7th Physical Simulation of Casting, Hot Rolling and Welding, Tsukuba, Japan, 21–23 January 1997; pp. 231–236.
42. Perttula, J.S.; Karjalainen, L.P. Recrystallisation rates in austenite measured by double compression and stress relaxation methods. *Mater. Sci. Technol.* **1998**, *14*, 626–630. [CrossRef]
43. Hodgson, P.D.; Gibbs, R.K. A mathematical model to predict the mechanical properties of hot rolled C-Mn and microalloyed steels. *ISIJ Int.* **1992**, *32*, 1329–1338. [CrossRef]
44. Sellars, C.M. Modelling microstructural development during hot rolling. *Mater. Sci. Technol.* **1990**, *6*, 1072–1081. [CrossRef]

45. Lang, V.; Suikkanen, P.; Somani, M.; Porter, D.; Karjalainen, P. Static recrystallization kinetics of austenite after hot deformation of carbide-free bainitic steels. In Proceedings of the International Science Technology Conference, St. Petersburg, Russia, 22–24 June 2011; pp. 301–304.
46. Ll, G.; Maccagno, T.M.; Bai, D.Q.; Jonas, J.J. Effect of initial grain size on the static recrystallization kinetics of Nb microalloyed steels. *ISIJ Int.* **1996**, *36*, 1479–1485. [CrossRef]
47. Somani, M.C.; Porter, D.A.; Hamada, A.S.; Karjalainen, L.P. High-temperature flow stress and recrystallization characteristics of Al-bearing microalloyed TWIP steels. *Metall. Mater. Trans. A Phys. Metall. Mater. Sci.* **2015**, *46*, 5329–5342. [CrossRef]
48. Cabañas, N.; Akdut, N.; Penning, J.; de Cooman, B.C. High-temperature deformation properties of austenitic Fe-Mn alloys. *Metall. Mater. Trans. A Phys. Metall. Mater. Sci.* **2006**, *37*, 3305–3315. [CrossRef]
49. Shen, W.; Zhang, C.; Zhang, L.; Xu, Q.; Cui, Y.; Xu, Y. A modified Avrami equation for kinetics of static recrystallization of Nb-V microalloyed steel: Experiments and numerical simulation. *Vacuum* **2018**, *150*, 116–123. [CrossRef]